ACS Catalysis

pubs.acs.org/acscatalysis Research Article

Cu^{II} Lewis Acid, Proton-Coupled Electron Transfer Mechanism for Cu-Metal−Organic Framework-Catalyzed NO Release from *S*-Nitrosoglutathione

Robert R. Tuttle, Richard G. Finke,* and Melissa M. Reynolds*

Cite This: *ACS Catal.* 2022, 12, 8055−8068 Read Online

ACCESS | Metrics & More | Article Recommendations | Supporting Information

ABSTRACT: Evidence is provided for a previously unknown proton-coupled electron transfer (PCET) mechanism for nitric oxide (NO) release from endogenous *S*-Nitrosoglutathione (GSNO) catalyzed by the metal−organic framework (MOF) $H_3[(Cu_4Cl)_3(BTTri)_8]$ (CuBTTri) in the presence of glutathione (GSH). The balanced reaction stoichiometry, active site characterization, and the experimental rate law are used to systematically disprove competing mechanistic hypotheses, leading unexpectedly to PCET as the proposed basic mechanism. The PCET mechanism contrasts traditionally proposed, either formally Cu^{II} to Cu^{I} redox or other formally Cu^{II} Lewis acid mechanisms for NO generation by other Cu-based catalysts. The proposed PCET mechanism sets the stage for mechanistically guided syntheses of improved Cu-MOF catalysts for GSNO to NO conversion and for computational investigations on the CuBTTri/GSNO/GSH/NO system as further tests of the well-defined structure of CuBTTri, structures of hypothesized reaction intermediates, and specific questions and hypotheses generated by the proposed PCET mechanism.

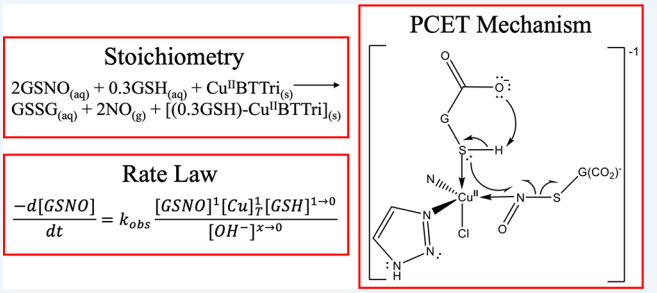

KEYWORDS: *kinetics and mechanism, heterogeneous catalysis, MOFs, nitric oxide, copper*

INTRODUCTION

CuBTTri: A MOF Catalyst for Biomedically Important Nitric Oxide Generation from Endogenous Sources. The catalytic generation of nitric oxide (NO) from endogenous sources such as *S*-Nitrosothiols (RSNO) by solid-state copper-based materials is important for implanted medical device applications.[1−5] Generating NO *in vivo* stimulates vasodilation for improved blood flow at medical device surfaces and increases the lifetime of implanted devices.[6−15]

One NO release system known to operate *in vivo* is generation of NO from the endogenous, nitrosated tripeptide *S*-Nitrosoglutathione (GSNO, Figure 1) in the presence of the corresponding thiol glutathione (GSH, Figure 1), catalyzed by the Cu-based metal−organic framework (MOF) $H_3[(Cu_4Cl)_3(BTTri)_8]$ (CuBTTri, Figure 2).[2,16−23] Glutathione disulfide (GSSG) has been established as the other main product of the reaction (Scheme 1)[22] for the CuBTTri/GSNO/GSH/NO system in water. CuBTTri is a promising MOF catalyst for biomedical application and NO generation from an endogenous source (GSNO) because CuBTTri is stable in biological media and is a solid-state catalyst that avoids problems with soluble Cu-based NO release catalysts, notably the acute liver toxicity associated with free Cu ions.[2,24] However, the prior lack of understanding of the reaction mechanism of CuBTTri-catalyzed conversion of GSNO to NO in the presence of GSH currently limits the most efficient use of such Cu-MOF NO release catalysts and inhibits any mechanism-directed design of future Cu-MOF catalysts with improved, mechanistically fine-tuned NO release properties.

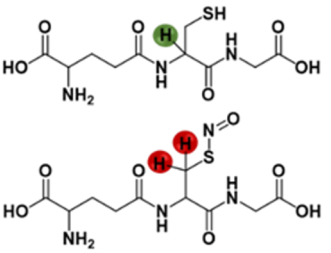

Figure 1. Structures and diagnostic protons used in ^1H NMR to detect and quantify GSH (green, top) and GSNO (red, bottom) in H_2O.

CuBTTri-Catalyzed GSNO to NO Conversion: The Reaction Stoichiometry and Thiol Dependence Estab-

Received: January 26, 2022
Revised: May 31, 2022

https://doi.org/10.1021/acscatal.2c00477
ACS Catal. 2022, 12, 8055−8068

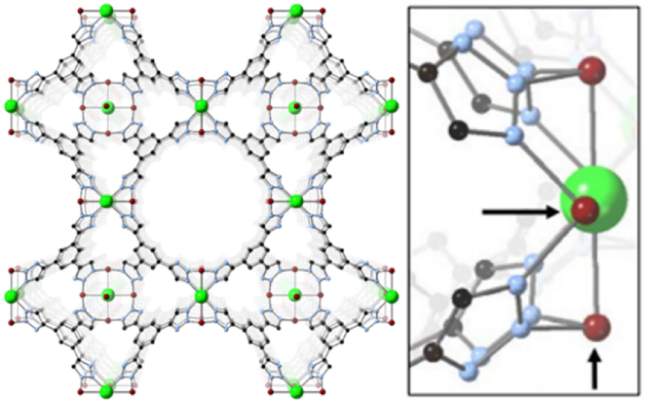

Figure 2. (Left) CuBTTri unit cell showing carbon (black), nitrogen (blue), chlorine (green), and copper (red). (Right) Finer, more detailed view of the nominally 3-coordinate $Cu_{surface}$ site (indicated with arrows) previously determined to be active for GSNO to NO conversion catalysis. The triazole linker suggested by the CuBTTri synthesis is illustrated in the finer view of the $Cu_{surface}$ site on the right.

Scheme 1. Balanced Reaction for GSNO to NO Conversion Catalyzed by CuBTTri Determined in Previous Work Which Showed That GSSG Is Formed Directly from GSNO[22,27a]

$$2GSNO_{(aq)} + 0.3GSH_{(aq)} + Cu^{II}BTTri_{(s)} \longrightarrow GSSG_{(aq)} + 2NO_{(g)} + [(0.3GSH)\text{-}Cu^{II}BTTri]_{(s)}$$

[a]Work from several groups, including our own, disproves the hypothesis that leached copper ions from the CuBTTri framework can be the source of GSNO to NO catalysis.[2,22,23,28−30]

lished in Prior Work. The balanced reaction stoichiometry for GSNO to NO conversion catalyzed by CuBTTri in H_2O has been previously established in an earlier paper and is shown in Scheme 1.[22] Investigating the reaction stoichiometry revealed that GSH must be added at stoichiometric levels to observe GSNO to NO catalysis by CuBTTri at a reasonable rate.[20,22] Without added GSH, only 10% loss of GSNO is observed over 16 h, but when one equivalent of GSH (relative to GSNO) is added, then 100% loss of GSNO is observed within 16 h, an apparent ∼10-fold acceleration of the reaction.[22] The dependence of CuBTTri on added GSH and the stoichiometry for NO release catalysis will turn out to be important in formulating mechanistic hypotheses consistent with the experimental evidence (*vide infra*).

We and others have hypothesized that Cu-catalyzed GSNO to NO conversion for both CuBTTri and solvated Cu ions operates through a mechanism involving a redox reaction at Cu and that GSH is critical in initiating that redox event.[23,25,26] Investigations into RSNO to NO conversion, at least as catalyzed by solvated copper ions, have led to the suggestion in the literature that the reduction of Cu^{II} to Cu^{I} is a necessary step for that particular reaction.[25,26] Poisoning experiments using the selective Cu^{I}-ion chelator neocuproine have been shown to halt the reaction completely when the solvated copper ion catalyst starts as Cu^{II}.[26] The Cu^{II} to Cu^{I} redox catalysis hypothesis for GSNO to NO conversion is, then, one that must be considered as a proposed mechanism for NO release from GSNO catalyzed by CuBTTri—electron transfer at or near the Cu site seemingly being required to generate a driving force for S−N bond homolysis.

Researchers have proposed that for other MOF-based systems, reaction mechanisms for solid-state MOFs and analogous homogeneous catalysts are the same, based for example, on identical observed reaction stoichiometries, a case in point being Ni-MOF-catalyzed ethylene dimerization.[31] However, the experimentally observed reaction stoichiometries are different for solid CuBTTri versus solvated Cu ion-catalyzed GSNO to NO conversion.[22] Specifically, the addition of stoichiometric levels of GSH to the reaction mixture is required to observe NO release catalysis for CuBTTri, but the opposite result is observed for solvated Cu ions—stoichiometric levels of GSH effectively poison Cu ion-catalyzed GSNO to NO conversion in H_2O.[18,22,25,32] Hence, the different stoichiometries and the different thiol dependencies for CuBTTri versus solvated Cu ion GSNO to NO conversion catalysis demand different reaction mechanisms for these two NO release catalysts.

Catalytically Active Cu Sites in CuBTTri for GSNO to NO Conversion. The active Cu sites in CuBTTri (synthesis shown in Scheme 2) for GSNO to NO conversion catalysis have been shown in our prior work to be (1) located on CuBTTri particle exterior surfaces; (2) low-coordinate, naturally occurring particle-termination $Cu_{surface}$ sites, which can bind 3 equivalents of cyanide per Cu site (Figure 2), and (3) present at just 1.3 ± 0.4% of the total Cu for CuBTTri particles 600 ± 400 nm in size.[23] Such low-coordinate, exterior-surface $Cu^{II}_{surface}$ sites should exhibit relatively low Marcus-type reorganization energy barriers (especially as compared to the 5-coordinate bulk intrapore Cu^{II} sites in CuBTTri) for any geometric rearrangement required for a Cu redox step, either a Jahn-Teller-distorted pseudo-octahedral Cu^{II} to tetrahedral Cu^{I} mechanism or, alternatively (and as our evidence will lead us to herein) for pseudo-octahedral, formally Cu^{II} sites in a ligand-based redox mechanism.[33,34] In short, the hypothesis that the surface active sites in CuBTTri are preferred for GSNO to NO conversion is at least consistent with, if not supported by, general Marcus theory considerations.

Scheme 2. Limiting Hypothetical Balanced Reaction for the Synthesis of CuBTTri in DMF[a]

$$8H_3BTTri_{(DMF)} + 12CuCl_2(H_2O)_{2(DMF)} \longrightarrow H_3[(Cu_4Cl)_3(BTTri)_8]_{(s)} + 21HCl_{(DMF)} + 24H_2O_{(DMF)}$$

[a]CuBTTri was synthesized and characterized following a previously reported procedure (more details are provided in the Experimental Section, *vide infra*).[29]

Another important feature of the CuBTTri active sites to introduce here (examined in greater detail in the Discussion section, *vide infra*) is the protonation state of the triazole moiety in the BTTri linker in the solid-state CuBTTri structure shown in Figure 2. The limiting stoichiometry for the CuBTTri synthesis (Scheme 2) and the original report of CuBTTri[29] suggest that Cu−N linkages are formed between Cu^{2+} cations and $BTTri^{3-}$ trianions. Therefore, it is implied that each triazole moiety is deprotonated in the dried, evacuated solid-state CuBTTri precatalyst (as illustrated in Figure 2). Without writing the balanced reaction stoichiometry for the CuBTTri synthesis (Scheme 2), one may not realize that the protonation state of the triazole moiety in BTTri could change upon formation of the MOF and under different reaction conditions (*vide infra*).

Minimum Requirements for Establishing a Reliable Ockham's Razor-Obeying Reaction Mechanism in any Catalytic System. It is useful at this point to list the five requirements that any experimentally determined reaction

https://doi.org/10.1021/acscatal.2c00477
ACS Catal. 2022, 12, 8055−8068

mechanism for a catalyst system should meet, at a minimum and ideally speaking.

1) The full catalytic reaction stoichiometry, including mass and charge balance.[22,35] A balanced reaction is critical in investigations of catalytic mechanisms.[36,37] Without a balanced reaction in hand, one cannot write the correct series of elementary steps that sum to the observed stoichiometry, so that the possibility then exists of proposing a mechanism that is simply incorrect because it is for another ("the wrong") reaction.
2) Determination of the kinetically dominant active site(s).[23,35,38−43] Active site investigation in MOFs, for example, will ideally determine the location and number and include some structural information about the active site(s).[44−46] Are, for example, MOF intrapore sites the catalytically active sites as in the traditional "MOF catalysis hypothesis" or, instead, are surface sites the true active sites?
3) Kinetics data must be obtained for all reactants present using direct physical handles if possible.[22] Comparing the experimentally observed rate law to rate laws derived for proposed mechanisms is an essential part of disproving or, if not, supporting competing mechanistic hypotheses.
4) Elementary (or pseudo-elementary[47]) steps, which sum to the observed balanced reaction, are required. These elementary or pseudo-elementary[47] steps define the rate constants for each step of the reaction. Elementary steps also eliminate any possible language-based confusion about reaction mechanisms by defining the concepts and associated language needed to describe the mechanism unequivocally via those steps.
5) Consideration and attempted disproof of multiple competing deliberately minimalistic mechanistic hypotheses.[48] Initial mechanistic hypotheses should only contain the minimal elementary steps and assumptions necessary to explain all data; that is, proposed mechanisms should obey Ockham's razor.[49]

Previous work discussed earlier in this introduction (Figures 1 and 2, Scheme 1) has satisfied requirements 1 and 2 in the above list.[22,23] Specifically, balanced reaction stoichiometry (Scheme 1) and the Cu active sites (Figure 2) are known for CuBTTri-catalyzed GSNO to NO conversion in the presence of added GSH. The previously unsatisfied requirements to a reliable initial mechanism, 3, 4, and 5 in the above list, are what the present work strives to address for the CuBTTri/GSNO/GSH/NO system.

Focal Points Herein Addressing the Mechanism of NO Release Catalysis. Herein, we report the experimental rate law for CuBTTri-catalyzed GSNO to NO conversion with respect to GSNO, GSH, total Cu, and pH. We considered six main competing mechanistic hypotheses that made sense *a priori* (two formally Cu^{II} Lewis acid mechanisms, three formally Cu^{II} to Cu^{I} redox mechanisms, and one again formally Cu^{II} to Cu^{III} mechanism). Of course, as is always the case in studying reaction mechanisms, the hypotheses considered initially are chosen from a list constructed from the literature, from what is deemed reasonable using one's knowledge of the system of interest,[48,49] as well as from one's broader chemical and mechanistic knowledge. Looking ahead to a summary of what follows, a disproof-based, currently favored proposed mechanistic hypothesis will be provided in the Discussion section. To the best of our knowledge, few if any prior studies of a MOF-catalyzed reaction fulfill all five of the requirements listed previously en route to a more reliable minimum reaction mechanism.[36,37,50] This is despite the significance of kinetic and mechanistic studies of MOF catalysts to enable reliable mechanism-directed design of improved catalysts via the unparalleled chemical and physical tunability of MOFs[44,51−54] among the approaching 10^6 unique MOF structures presently known.[55]

EXPERIMENTAL SECTION

Reagents. Diethylamine (99%), trimethylsilylacetylene (98%), trimethylsilylazide (94%), and 1,3,5-tribromobenzene (98%) were purchased from Alfa Aesar (Ward Hill, MA, USA). Glutathione (98%) was purchased from VWR (Radnor, PA, USA). Sodium nitrite (99.5%), copper(I) iodide (99.5%), bis(triphenylphosphine)palladium(II) dichloride (99%), dichloromethane (99%), and monobasic sodium phosphate (≥98%) were purchased from Sigma-Aldrich (St. Louis, MO, USA). HCl (1 N), methanol (99%), and sodium hydroxide (98.9%) were purchased from Fisher Scientific (Hampton, NH, USA). Dimethylformamide (99%) and copper(II) chloride dihydrate (99%) were purchased from EMD Chemicals (Gibbstown, NJ, USA). 2-(*N*-Morpholino)ethanesulfonic acid (MES) (99%) was purchased from VWR (Radnor, PA, USA). Piperazine-*N*,*N*′-bis(3-propanesulfonic acid) (PIPPS) (≥97%) was purchased from MilliporeSigma (Burlington, MA, USA). Ultrahigh-purity nitrogen gas (99%) was supplied by Airgas (Denver, CO, USA). Deionized water (18.2 MΩ·cm) was obtained from a Millipore Direct-Q water purification system (EMD Millipore, Billerica, MA, USA). All materials were used as received without any further purification.

GSNO Synthesis. GSNO was prepared, and its purity verified, following an established literature protocol (Scheme 3).[56] Briefly, a solution of glutathione (1.60 g, 5.21 mmol) was

Scheme 3. Synthesis of GSNO from GSH

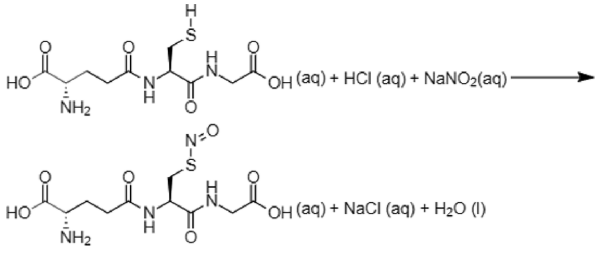

prepared in Millipore filtered water (8 mL) containing 2 M HCl (2.5 mL, 10.5 mL total volume). One equivalent of sodium nitrite (0.361 g, 5.21 mmol) was added, and the resulting mixture was stirred for 40 min at 5 °C. Acetone (10 mL) was added to the resulting red solution, and the mixture was stirred for another 10 min. The red precipitate was collected via vacuum filtration and washed with ice-cold water (5 × 5 mL) and ice-cold acetone (3 × 10 mL). The precipitate was then dried on a high vacuum line for 4 h to afford *S*-Nitrosoglutathione (1.43 g, 4.22 mmol, 81%) (λ_{max}) (H_2O) 335, 550 nm (ε = 922 cm^{-1} mM^{-1}). The GSNO sample used herein was determined to be (97 ± 2) % pure by UV−VIS spectroscopy. The GSNO sample used to collect the data reported herein comes from the same batch of GSNO used in previously published work.[23] The small, 3 ± 2%, impurity present in the GSNO is glutathione (GSH) leftover from or glutathione disulfide (GSSG) generated from the GSNO synthesis. Relevant here is that previous work on

https://doi.org/10.1021/acscatal.2c00477
ACS Catal. 2022, 12, 8055−8068

Scheme 4. Coupling Aryl Halide and Trimethylsilylacetylene

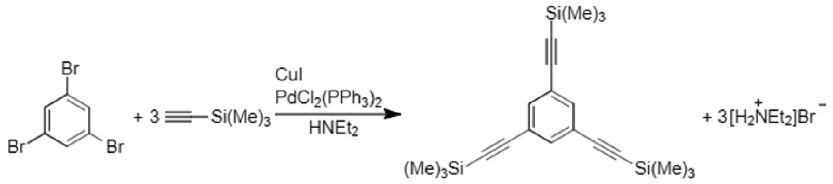

GSNO to NO conversion catalyzed by CuBTTri established that GSH must be present to initiate measurable CuBTTri-catalyzed GSNO to NO conversion within 20 min.[22,32]

H_3BTTri Ligand Synthesis. The H_3BTTri ligand was prepared and characterized following an established literature protocol (Schemes 4−6).[29] Briefly, solid 1,3,5-tribromobenzene (9.45 g, 30.0 mmol) was dissolved in diethylamine (250 mL) under inert conditions (N_2). Copper(I) iodide (50 mg, 0.26 mmol) and dichlorobis(triphenylphosphine)palladium(II) (400 mg, 0.57 mmol) were added to the stirred solution. Trimethylsilylacetylene (10.6 g, 108 mmol) was added to the solution, and the resulting mixture was heated at 50 °C for 6 h. The resulting diethylamine hydrobromide was removed by filtration and washed with ether (45 mL). Combined washings were evaporated to dryness in vacuo at 30 °C, and the resulting product was purified by a silica plug to yield 9.61 g (78%) 1,3,5-tris(trimethylsilylethynyl)benzene as an intermediate. ^{1}H NMR (400 MHz, $CDCl_3$): δ = 7.43(s), 0.23(s) ppm.

Scheme 5. Hydrolysis of the Trimethylsilylethynyl Intermediate

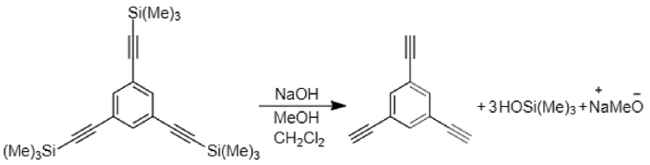

Scheme 6. Click Reaction to Form 1,3,5-tris(^{1}*H*-1,2,3-triazol-5-yl)benzene

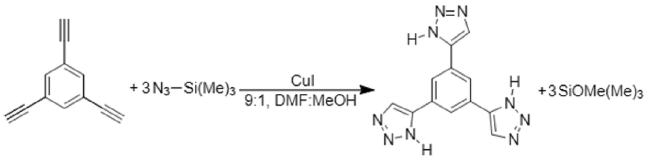

The 1,3,5-tris(trimethylsilylethynyl)benzene intermediate (9.61 g, 26.3 mmol) was hydrolyzed by treatment with NaOH (aq) (30 mL, 1 M), CH_2Cl_2 (20 mL), and methanol (50 mL) via stirring at room temperature for 3 h. Evaporation of methanol, extraction of the residue by ether, and evaporation of the solvent in vacuo at 30 °C yielded 2.68 g of white powder containing 1,3,5-triethynylbenzene. ^{1}H NMR (400 MHz, $CDCl_3$): δ =7.51(s), 3.12(s) ppm.

Trimethylsilylazide (9.26 g, 80.4 mmol) was added to a solution of copper(I) iodide (510 mg, 2.63 mmol) and 1,3,5-triethynylbenzene (2.68 g, 17.8 mmol) under N_2 gas in a mixture of dimethylformamide (DMF; 90 mL) and methanol (10 mL). The resulting mixture was heated to 100 °C using a hot plate and stirred for 36 h. The mixture was then filtered using a vacuum filter and filter paper and reduced to a volume of 10 mL via rotary evaporation at 30 °C. A pale-yellow precipitate was formed upon the addition of Millipore filtered water (30 mL) to the resulting filtrate. The solid was collected by filtration, washed with ether, and dried in vacuo to yield 4.1 g (83%) of 1,3,5-tris(^{1}*H*-1,2,3-triazol-5-yl)benzene. ^{1}H NMR (400 MHz, $(CD_3)_2SO$): δ = 8.52(s), 8.34(s) ppm. The H_3BTTri used in this work is from the same batch prepared and used in two previous publications.[21,24]

CuBTTri Synthesis. CuBTTri was synthesized and characterized following a previously reported procedure (Scheme 2).[29] A solution of H_3BTTri (225 mg, 0.937 mmol) in DMF (40 mL) was prepared in a 250 mL Pyrex bottle. $CuCl_2{\cdot}2H_2O$ (383 mg, 2.25 mmol) was added to the solution. The vial was heated at 100 °C for 72 h in an oven to afford $H_3[(Cu_4Cl)_3(BTTri)_8(DMF)_{12}]{\cdot}7DMF{\cdot}76H_2O$. The purple powder was washed with boiling DMF (10 × 10 mL), and DMF was allowed to evaporate under ambient conditions for 18 h to yield 218 mg (76%) of product. Solvent exchange was performed using a Soxhlet extractor and Millipore filtered water to yield $H_3[(Cu_4Cl)_3(BTTri)_8(DMF)_{12}]{\cdot}72H_2O$. The resulting light-purple powder was hand-ground for 5 min, gravity-filtered through 1 μm mesh, and analyzed by powder X-ray diffraction (pXRD). The batch of CuBTTri used to collect the data reported herein comes from the same batch used in previously published work.[23] The observed diffraction pattern matched a literature standard (Figure S1).[29]

Buffered Reactions. Measuring the reaction rate at different pH levels required that the reaction solutions be buffered to specific pH values. These experiments required the use of a buffer that would not coordinate to the Cu sites in CuBTTri; hence, we chose to use buffers of *N*,*N*′-bis(3-propanesulfonic acid) (PIPPS) or 2-(*N*-morpholino)ethanesulfonic acid (MES).[26] The buffered solutions were prepared by dissolving solid PIPPS or MES powders in Millipore water to achieve a 0.5 M solution. Then, a 10 N NaOH solution was added dropwise to the PIPPS or MES buffer solution until the desired pH was achieved. The buffered PIPPS or MES solutions were then used to prepare GSNO and GSH solutions from solid GSNO or GSH powder. These solutions were then used in an identical reaction procedure to the one described below to measure the reaction rate at different pH levels. All the reaction rate versus pH studies were carried out under conditions where the reaction was saturated in [GSH] (*vide infra*). Therefore, the Cu active sites available were coordinated with GSH (*vide infra*).

Reaction Procedure. All reactions described herein were carried out under an N_2 (g) atmosphere to minimize the presence of O_2 (g) in the reactions. GSNO and GSH solutions were prepared using Millipore H_2O and solid GSNO or GSH under inert conditions (N_2) in a 200 mL round-bottom flask capped with a rubber septum and flushed with N_2. CuBTTri (600 ± 400 nm octahedral particles) was massed into a three-neck 100 mL round-bottomed flask and oven-dried overnight at 110 °C. The CuBTTri samples used in this work are the same batch of particles previously employed in prior work.[23] Following the oven drying, the flask containing CuBTTri was placed under vacuum for 1 h on a Schlenk line and backfilled with N_2(g) prior to reaction. GSNO or GSH solutions were then

https://doi.org/10.1021/acscatal.2c00477
ACS Catal. 2022, 12, 8055−8068

injected into the reaction flasks containing the dried CuBTTri. For buffered reactions, the GSNO or GSH solutions were prepared using buffered Millipore H_2O. Vigorous bubbling in the round-bottom flask was established using an inlet $N_2(g)$ flow needle and an outlet needle. Reactions were bubbled vigorously to mitigate mass transport limitations and to ensure that the measured value for $[-d[GSNO]/dt]_i$ was not simply the rate of substrate diffusion to the MOF active sites.[57,58] Reaction flasks were completely covered in aluminum foil to minimize exposure to light, and reactions were left to proceed for a predetermined time. The outlet needle was removed to stop bubbling at a predetermined time, and once all visible CuBTTri particles had settled to the bottom of the flask (~30 s), the supernatant was decanted via a syringe. The quenched reaction solution was then kept cool and in the dark in an EPA-certified Cu-free glass vial under inert conditions (N_2) or added directly to an NMR tube or UV−VIS quartz cuvette within less than 1 min. ^{1}H NMR or UV−VIS spectra were collected at 20 min to allow sufficient loss of GSNO to be detectable, yet to remain relatively early in the reaction progress to determine what is designated as an initial rate ($-d[GSNO]/dt$). Practically and given the approximately ±5% precision of the ^{1}H NMR data under our conditions, the tradeoff between measurable reaction vs more points meant that taking 1 point in the first ~30% reaction was a good compromise that allowed reasonable initial rate measurements. ^{1}H NMR and UV−VIS spectroscopy techniques have been determined to be equivalent techniques for monitoring loss of GSNO in the current system. All reactions reported were performed in triplicate with the reported average and standard deviation calculated from those three trials.

Water Suppression ^{1}H NMR. These experiments follow our protocol for direct *in situ* monitoring the release of NO from GSNO in water by solvent-suppressed ^{1}H NMR.[22] All NMR experiments were performed using an Agilent Inova 500 equipped with a 5 mm pulsed-field-gradient HCN probe. Samples were prepared in septa-capped Wilmad 528−PP 500 MHz tubes under inert conditions (N_2) by adding 0.5 mL of reaction supernatant to an NMR tube containing 0.1 mL of 20 mM NaH_2PO_4-buffered D_2O. Samples were mixed by hand followed by 2 s of sonication to remove N_2 bubbles. Samples were kept in the dark and air-free and analyzed as soon as possible, typically within 5 min. NMR experiments were run using PRESAT with PURGE solvent signal suppression available in VnmrJ version−4.2.[59] The system was buffered with NaH_2PO_4 due to the sensitivity of the compounds of interest (GSNO, GSH, and GSSG) to the pH of the solution. 512 transients were acquired for all samples, which required 35 min. A 2 s square presat with a bandwidth of 100 Hz on resonance at 4.67 ppm (water) was used followed by the PURGE crusher sequence and a $\pi/2$ excitation pulse of 5.7 μs. Acquisition time was 2 s, and with the PRESAT delay, the total time between transients was about 4 s. All free induction decay (FID) spectra were processed using MestraNova software to examine peak intensities and integration values. Data analysis and calculations were performed using Microsoft Excel and OriginPro.

RESULTS

Previous work on CuBTTri-catalyzed GSNO to NO conversion satisfied requirements 1 and 2 as listed in the Introduction en route to a more reliable minimum reaction mechanism (*vide supra*) by, respectively, (1) determining the balanced reaction stoichiometry (Scheme 1) and (2) providing compelling evidence for exterior surface Cu sites in the CuBTTri/GSNO/GSH/NO system as the kinetically dominant, catalytically most active sites (Figure 2).[23] Hence, we turned our efforts toward requirement 3, namely, obtaining experimental kinetics data for the rate law with respect to [GSH], [GSNO], $[Cu]_T$, and, as we will see, the informative effects of the reaction pH.

Figure 3 shows the first-order integrated rate plot for $\ln[GSNO]_t$ vs the reaction time. [GSNO] was monitored in

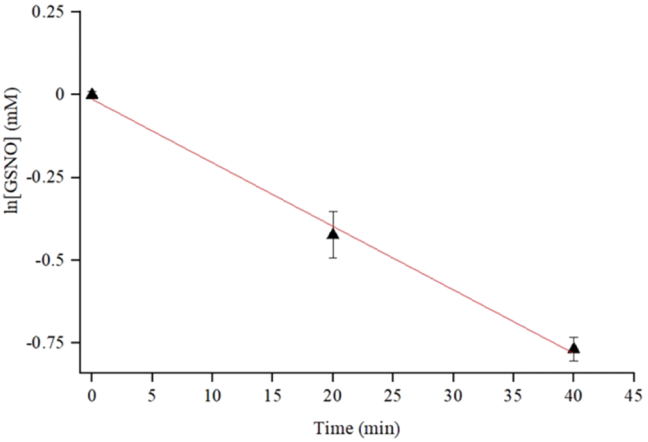

Figure 3. First-order integrated rate plot of $\ln[GSNO]_t$ versus time when $[GSNO]_i$ = 1 mM. The linear trend line is fit by the equation $y = ((-1.92 \pm 0.11) \times 10^{-2})x - ((1.32 \pm 2.94) \times 10^{-2})$, R^2 = 0.99. The reaction is first-order in GSNO at 1 mM and at 20 min reaction time (for the standard reaction conditions described herein).

H_2O using the previously reported solvent suppression ^{1}H NMR method.[22] Figure 3 shows that the reaction is first-order in [GSNO] under the standard reaction conditions reported herein (i.e., when $[GSNO]_i$ is 1 mM). Additional data were collected where $[GSNO]_i$ = 1.5 and 2 mM and 0th and 2nd-order integrated rate plots were generated for further analysis of the reaction dependence on [GSNO] (full details in Figure S2). The linear fit of the data where $[GSNO]_i$ = 1 mM yields the empirical rate law (eq 1):

$$\frac{-d[GSNO]}{dt} = k_{GSNO,obs}[GSNO]^1 \quad (1)$$

where $k_{GSNO,obs}$ is the observed first-order rate constant $(1.92 \pm 0.11) \times 10^{-2}$ s^{-1}.

Next, Figure 4 shows the relationship between the reaction rate ($-d[GSNO]/dt$) and the initial concentration of GSH added to NO release reactions with CuBTTri. The reaction is 1st-order in [GSH] in the lower range of concentrations studied (0.025 to 0.15 mM, first four points in Figure 4). For higher levels of [GSH], the reaction becomes 0th-order in [GSH], that is, exhibits saturation kinetics in [GSH]. A linear fit of the 1st-order portion of the plot (the first four points) in Figure 4 yields the empirical rate law, eq 2, where $k_{GSH,obs}$ is $(1.8 \pm 0.1) \times 10^{-3}$ s^{-1}.

$$\frac{-d[GSNO]}{dt} = k_{GSH,obs}[GSH]^{1\rightarrow 0} \quad (2)$$

Third, Figure 5 shows the relationship between $-d[GSNO]/dt$ and the amount of exterior surface Cu sites in CuBTTri (reported as mol % of GSNO). Previous work has shown that the NO release reaction is first-order in the CuBTTri particle exterior surface area.[23] The plot in Figure 5 shows that the reaction is first-order in catalytically active $Cu_{surface}$ sites. The

https://doi.org/10.1021/acscatal.2c00477
ACS Catal. 2022, 12, 8055−8068

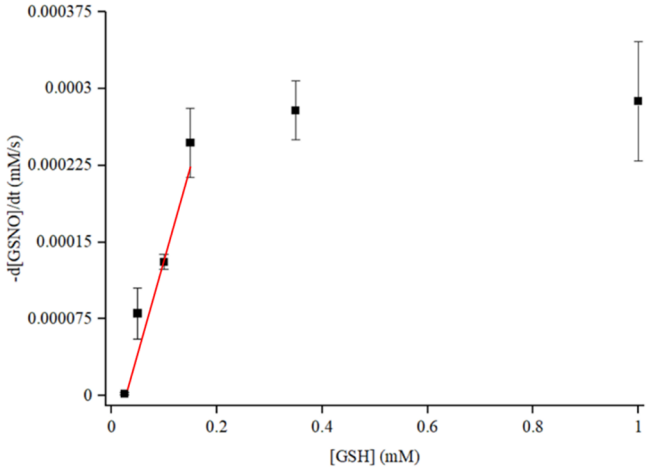

Figure 4. Plot of $-d[GSNO]/dt$ measured at 20 min reaction time versus $[GSH]_i$ added to the reaction mixture. There are two distinct domains shown in this plot: in the first domain, the reaction appears first-order in [GSH]; in the second domain, the reaction is zero-order in [GSH], overall showing saturation kinetics with respect to [GSH]. The first point of the plot corresponds to a set of experiments where no GSH was added to the reaction, so that the only ~3% GSH present ([GSH] = 0.025 mM) is an impurity from the GSNO synthesis (as summarized in the Experimental section). All other experiments and points past [GSH] = "0" contain added GSH beyond that baseline impurity level. The trend line where the reaction is 1st-order in [GSH] is fit by the equation $y = ((1.8 \pm 0.1) \times 10^{-3})x - ((4.2 \pm 0.29) \times 10^{-5})$, $R^2 = 0.99$, from linear least squares. Physically, the intercept cannot be negative ($-(4.2 \pm 0.29) \times 10^{-5}$ mM s^{-1}), so that the error at 3 sigma is taken to be $(\pm(1.2 \pm 0.09)) \times 10^{-4}$ mM s^{-1}. An important part of this plot is its zero intercept within experimental error; that is, the reaction does not occur unless GSH is present.

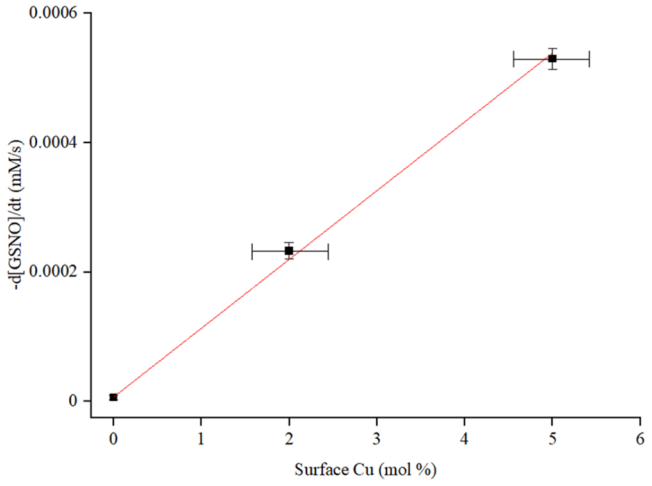

Figure 5. Plot of $-d[GSNO]/dt$ measured at 20 min of reaction versus $Cu_{surface}$ sites added into the reaction (Cu reported as percentage of mol GSNO). The line is fit by the equation $y = ((1.06 \pm 0.04) \times 10^{-4})x + ((6.74 \pm 3.98) \times 10^{-6})$, $R^2 = 0.99$. The horizontal error bars represent the previously determined experimental error in the active site density of the CuBTTri particles used herein. High CuBTTri mass loadings required for greater than 5 mol % $Cu_{surface}$ resulted in artificially lowered experimental $-d[GSNO]/dt$, apparently due to mass-transport limitations in the turbid, suspended-solid solution.

number of $Cu_{surface}$ sites present in each experiment was calculated using the previously determined Cu active site density in 600 ± 400 nm CuBTTri particles.[23] The linear relationship in Figure 5 yields the empirical rate law for just the Cu-catalyst component, eq 3:

$$\frac{-d[GSNO]}{dt} = k_{Cu,obs}[Cu_{surface}]^1 \quad (3)$$

The observed first-order rate constant, $k_{Cu,obs}$, set by the slope of the line in Figure 5 is $k_{Cu,obs} = (1.06 \pm 0.04) \times 10^{-4}$ s^{-1}. The $[Cu_{surface}]$ term in eq 3 reflects the total number of $Cu_{surface}$ sites, that is, the "concentration" of insoluble Cu sites suspended in the volume of solution by vigorous stirring, as detailed in the Experimental section.

Figure 6 shows $-d[GSNO]/dt$ as a function of reaction pH in buffered solutions prepared using non-coordinating buffers over

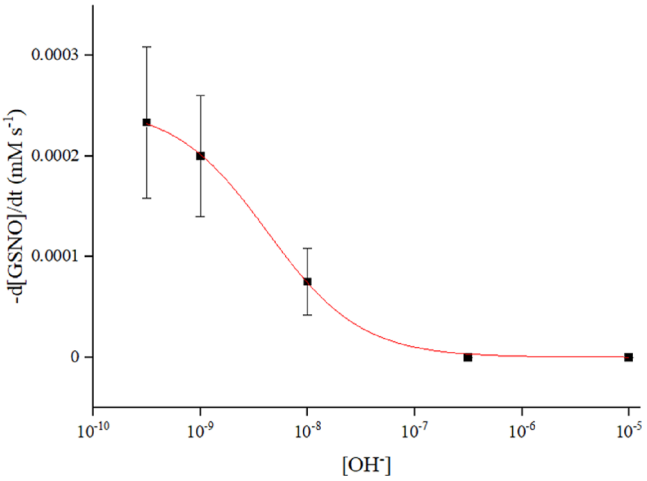

Figure 6. Plot of $-d[GSNO]/dt$ versus $[OH^-]$. The x axis is presented on a $\log_{10}$ scale necessitated by the fact that the $[OH^-]$ was varied by 4.5 orders of magnitude. At pH = 9 (furthest right point), the measured value of $-d[GSNO]/dt$ = 0 mM s^{-1}, and closer analysis of the data implies that when pH ≥ ~6.7, $-d[GSNO]/dt$ = 0 mM s^{-1} occurs. The data has been fit using non-linear least squares and a Levenberg–Marquardt iteration algorithm to an equation derived from the proposed mechanisms, specifically the equation $y = A/(1 + Bx)$ were A and B will be combinations of mechanism-based rate and/or equilibrium constants, $A = (2.50 \pm 0.2) \times 10^{-4}$ s^{-1} and $B = (2.38 \pm 0.01) \times 10^8$ M^{-1}. The values for A and B were not constrained in the fitting nor did the estimates for A and B change significantly if the data points were weighted equally or by their relative standard deviations. The data allow estimation of the pK_a of the proton being titrated with OH^-, p*K*a ~5.6 as detailed in the Supporting Information (Calculation S2). Derivation of the fitting equation used, and further analysis and discussion of the results shown in the plot above are presented in the Discussion section (*vide infra*).

4.5 orders of magnitude in $[OH^-]$ and under conditions zero-order in [GSH], as detailed in the Experimental section. The observed decrease in $-d[GSNO]/dt$ as reaction pH increases implies that OH^- is involved in catalyst deactivation. Relevant here is that GSNO and GSH are endogenous tripeptides with multiple exchangeable carboxylate and thiol protons (Figure 1, *vide supra*), but where both $-CO_2H$ protons are already removed at the pH values in Figure 6 so that the −SH proton in GSH is the only one left (in at least GSH or GSNO) that could be deprotonated in the experiments summarized in Figure 6. Additionally, the protonation state of the triazole moiety in the BTTri linker might also explain the observed loss of catalytic activity in Figure 6 at alkaline pH. More specifically, the hypotheses for the observed pH dependence are that (1) Cu^{II}-

https://doi.org/10.1021/acscatal.2c00477
ACS Catal. 2022, 12, 8055−8068

Table 1. Considered, but Disproved, Mechanistic Hypotheses[a]

		Specific Requirements for CuBTTri Catalyzed GSNO to NO Conversion Established Herein			
		A) Can this hypothesis be written to sum to the observed reaction stoichiometry?	B) Does this hypothesis make use of the previously characterized Cu active sites?	C) Does the derived rate law for this hypothesis match what is observed experimentally?	D) Can this hypothesis be written as a reasonable, minimalistic catalytic cycle?
Mechanistic Hypothesis	1) Cu^{II} Lewis acid, NO release resulting from inductive effects	✓	✓	✗	✗
	2) Cu^{II} Lewis acid, thiol coupling	✗	✓	✗	✓
	3) Cu^{II} to Cu^{I} redox, GS^- is the reductant	✗	✓	✗	✓
	4) Cu^{II} to Cu^{I} redox, GS• forms from GSH	✗	✓	✓	✗

[a]The requirements listed at the top of the second through fifth columns in Table 1 are the requirements for a reliable mechanism determination in this system, A–D, listed at the end of the Results section. Each disproved hypothesis fails to satisfy at least two of the four requirements A–D, thereby disproving all four listed mechanisms based on the current data. These four hypotheses correspond to Schemes S4–S7, respectively, in the Supporting Information.

bound GSH, (Cu^{II}-S(***H***)G), is being deprotonated and Cu^{II}-(S^-)G is a poisoned form of the catalyst, (2) a Cu^{II}-bound protonated triazole moiety (Cu^{II}-N_2(N**H**)C_2) is being deprotonated and Cu^{II}-N_2(N^-)C_2 is a poisoned form of the catalyst, or (3) a combination of both deprotonation events is required to explain the observed catalyst poisoning in Figure 6. These hypotheses will be examined in the upcoming Discussion section. Figure 6 also suggests that the catalysis observed herein requires an exchangeable proton (of pK_a ∼ 5.6, Supporting Information, Calculation S2) be present throughout the reaction and that the necessary proton exchange may not proceed through protons or hydroxide ions (i.e., the mechanism studied herein may involve general, and not specific, acid–base catalysis, *vide infra*).[60]

Overall, the kinetics data reported in Figures 3–6 reveal that the rate law for CuBTTri-catalyzed GSNO to NO conversion is (a) first-order in [GSNO], (b) first-order initially in [GSH], but then goes to zero-order (saturation kinetics) in [GSH], (c) first-order in [$Cu_{surface}$] sites, and (d) inversely dependent on [OH^-], varying from an initial, "inverse *x*-order" dependence ($x \sim 1$) to a zero-order dependence at higher [OH^-]. The kinetics data herein yield the experimental rate law shown in eq 4 under the assumption that the reaction mechanism does not change when moving from pH = 4.5 to 6 to 9, a point we will return to in the Discussion section and a quite reasonable assumption given that the data will point to only two proton sites that may be affected, the thiol proton in GSH[61] and more specifically in Cu^{II}-S(***H***)G or the triazole proton in Cu^{II}-N_2(N**H**)C_2.

$$\frac{-\mathrm{d[GSNO]}}{\mathrm{d}t} = k_{obs}\frac{[\mathrm{GSNO}][\mathrm{Cu_{surface}}][\mathrm{GSH}]^{1\to 0}}{[\mathrm{OH^-}]^{x\to 0}} \quad (4)$$

At constant pH = 4.5 where the bulk of the catalysis and kinetics were measured, the apparent rate law simplifies to eq 5, where the small, constant denominator [OH^-]$^{-x}$ term has been absorbed into k'_{obs}:

$$\frac{-\mathrm{d[GSNO]}}{\mathrm{d}t} = k'_{obs}[\mathrm{GSNO}][\mathrm{Cu_{surface}}][\mathrm{GSH}]^{1\to 0} \quad (5)$$

Equations 4 and 5 satisfy the 3rd requirement for determining a catalytic reaction mechanism (*vide supra*), namely, obtaining an experimental rate law for the observed reaction under a range of experimental conditions, including pH.

A Summary of the Key Experimental Evidence that Must Be Accounted for by Any Proposed Initial Minimum Mechanism. The Results section herein combined with our prior work[22,23] establishes four key pieces of evidence that any proposed GSNO to NO catalytic cycle for the CuBTTri/GSNO/GSH/NO system must meet.

A. The proposed mechanism must of course sum to the experimentally observed reaction stoichiometry (Scheme 1, *vide supra*).

B. The proposed mechanisms must operate via the previously characterized $Cu_{surface}$ active sites on CuBTTri (Figure 2). Those catalytic $Cu_{surface}$ sites have 3 open coordination sites to accept ligands other than solvent and are bound to two nitrogen atoms from the H_3BTTri linker and one interstitial chlorine atom.[28−30] The $Cu_{surface}$ active sites can be poisoned by cyanide, by the bulky ligand 3,3′,3″-phosphanetriyltris(benzenesulfonic acid)-trisodium salt (TPPTS), and the results herein reveal poisoning by abstraction of protons available in the catalytic cycle by OH^- (*vide infra* and *vide supra*).[23] Previously reported results detail the following *evidence inconsistent with freely diffusing Cu ions* as being the kinetically dominant catalyst: (i) the lack of catalytic activity of the reaction supernatant; (ii) solvated Cu ion poisoning by GSH; (iii) catalyst poisoning by the bulky ligand TPPTS; and (iv) the surface sites detected by FT-IR spectroscopic analysis of CuBTTri poisoned by cyanide. A more detailed discussion of these four points can be found in the Supporting Information.[1,2,22]

C. The mathematically derived rate law for proposed mechanisms must match the experimentally observed rate law provided in eqs 4 and 5; and

D. The proposed mechanism must be able to be written as a catalytic cycle, so that for example after NO release from

https://doi.org/10.1021/acscatal.2c00477
ACS Catal. 2022, 12, 8055−8068

Scheme 7. Proposed Mechanism and Catalytic Cycle for GSNO to NO Conversion Catalyzed by CuBTTri in Water[a]

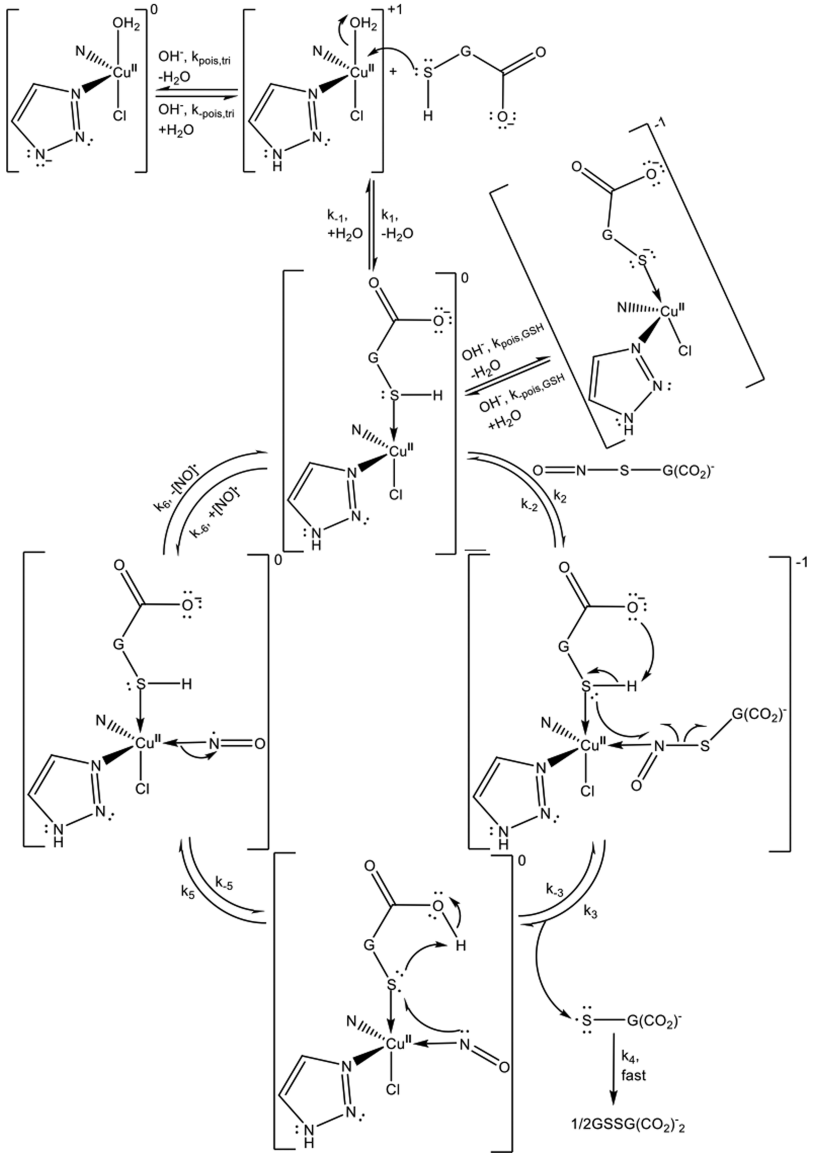

[a]Steps 1 and 2 (rate constants k_1/k_{-1} and k_2/k_{-2}) are GSH and GSNO coordination to the formally Cu^{II} pre-active site. Step 3 (rate constants k_3/k_{-3}) is ligand-based PCET between GSH and GSNO. We point out here that the intramolecular deprotonation proposed in Step 3 may be an oversimplification/representation of what, instead, is a Grotthus-type proton hopping mechanism involving one or more water molecules,[72] for example in the case where precise wrap-around of the $-COO^-$ to the Cu-(S^+(*R*)-H) as shown in this scheme is not possible. In addition, the "intermediate" at the bottom of Scheme 7 (i.e., after the k_3 step) is implied to be short-lived, and potentially closer to a transition state structure because the -G(CO_2**H**) proton (pK_a ~2.1 - 3.5) will be lost to the pH = 4.5 reaction solution at a diffusion-controlled rate. Step 4 (rate constant k_4): GSSG formation. Steps 5 and 6 (rate constants k_5/k_{-5} and k_6/k_{-6}) close the catalytic cycle by ligand-based PCET from $[NO]^-$ back to GSH. The formal oxidation state of Cu^{II} remains unchanged throughout the cycle, and Cu^{II} (d^9) acts as a Lewis acid for ligand-based e^- transfer between S (in the GSH ligand) and N (in the GSNO ligand). Note that while each GSH/GSNO molecule contains two terminal carboxylate groups (Figure 1), only one has been shown in this scheme for the sake of simplicity and because only one carboxylate is involved in the proposed mechanism. The character "G" in the GSH and GSNO structures represents the identical tripeptide backbone in each molecule. Catalyst poisoning occurs via abstraction of the thiol proton in Cu^{II}-S(***H***)G by OH^-.

GSNO, the Cu active site must be back in the starting state where it then bound GSNO.

DISCUSSION

The following Discussion section contains four stages en route to establishing our suggested mechanism for CuBTTri-catalyzed GSNO to NO conversion. First, we provide a brief discussion of the alternative mechanistic hypotheses that have been considered, but which can be ruled out by the collected data. Second, we present the presently favored proposed mechanism and detail how it is consistent with and supported by the experimental rate law and other data. Key features of the catalytic cycle are then explained in more depth. The special properties of GSNO and GSH as substrates in the NO release reaction turn out to be an important part of that discussion—consistent with the literature where the endogenous tripeptides GSNO and GSH are known to exhibit unique behavior in comparison to other Cu/RSNO/RSH/NO release sys-

https://doi.org/10.1021/acscatal.2c00477
ACS Catal. 2022, 12, 8055−8068

tems.[17−20,25,26,32,62−67] Third, we will present specific hypotheses for and details about the catalyst poisoning observed at alkaline pH (Figure 6). Fourth, we present calculated values for important kinetic and thermodynamic parameters within the currently favored mechanistic hypothesis.

***A Priori* Reasonable, but Now Disproved, Alternative Mechanistic Hypotheses for CuBTTri-Catalyzed GSNO to NO Conversion in the Presence of GSH in H_2O.** The alternative mechanistic hypotheses we considered, but which can be ruled out, are summarized in Table 1. Disproven mechanisms are described briefly here and in greater detail (along with their arrow pushing schemes) in the Supporting Information (Schemes S4−S7) for the interested reader. A noteworthy point regarding Table 1 is that 3 of the 4 disproved alternative mechanisms are ruled out by the observation that they fail to match the observed reaction stoichiometry, a finding consistent with our statement in the Introduction that the experimentally determined reaction stoichiometry is the first requirement of reliable mechanistic studies.

First, we considered and were able to rule out two Cu^{II} Lewis acid mechanisms for CuBTTri-catalyzed GSNO to NO conversion (entries #1 and #2 in Table 1). Two other mechanistic hypotheses we considered are versions of the prevailing, supported Cu^{II} reduction to Cu^{I} hypothesis for solvated Cu ion-catalyzed GSNO to NO conversion to see if it could explain our observed stoichiometry and kinetics.[4,26,62,67−69] Those mechanisms, too, are disfavored for reasons provided in Schemes S1 and S2. One general comment about any mechanism involving a Cu^{II} to Cu^{I} redox change and an intrapore Cu site within the solid framework is as follows: a large and probably prohibitive Marcus intrinsic barrier is expected for any pseudo-octahedral Cu^{II} to tetrahedral Cu^{I} redox pathway and associated ∼6 to 4 coordinate geometry change. Indeed, it was Marcus theory considerations that led us to test for and find evidence of exterior surface Cu site catalysis in a prior paper.[23]

The Currently Favored, Proton-Coupled Electron-Transfer Mechanism Involving a Formally Cu^{II} Lewis Acid, Ligand-Based Redox Pathway. To our surprise, we eventually wound up with the formally Cu^{II} Lewis acid, ligand-based redox proton-coupled electron-transfer (PCET) mechanism in Scheme 7 as our proposed catalytic cycle for GSNO to NO conversion catalyzed by CuBTTri (i.e., at the end of our studies and after consideration of literature hypotheses or other reasonable mechanisms). PCET is the minimal explanation consistent with the available data and that also provides a reasonable driving force for S−N bond homolysis (e.g., with the data in Figure 6 revealing that proton transfer is necessary to observe catalysis). PCET is also favored because inductive effects alone from a simple Cu^{II} Lewis acid mechanism (Scheme S4) are, in our opinion, insufficient to explain the observed S−N bond homolysis. The Cu^{II} precatalyst site starting/resting state in Scheme 7 is drawn and written as Cu^{II}-$N_2(NH)C_2(N)(Cl)$-(OH_2) to reflect the hypothesis that each $Cu^{II}_{surface}$ site (Figure 2) is coordinated to one chlorine atom and two separate triazole moieties (one triazole moiety has been omitted and replaced by a single N atom for simplicity).[28−30] The triazole moiety is currently written as $N_2(NH)C_2$ to reflect what is expected to be protonated at pH = 4.5, where the bulk of the kinetics data was collected (this point is discussed in greater detail below, *vide infra*).[28−30] We note here that the precatalyst site is formally a net +1 complex at pH = 4.5, at least locally, as indicated by the "$[\ ]^{+1}$" nomenclature around the species at the top of Scheme 7. The structures in the catalytic cycle are drawn with a trigonal-bipyramidal geometry because steric effects resulting from the bulky nature of the GSH/GSNO tripeptide ligands (Figure 1) are likely minimized by placing one tripeptide in an axial position and the other in an equatorial position. Metal complexes with d^9 electron counts, as in a formally Cu^{II} site in Scheme 7, are known to exhibit little to no structural preference energy for D_{3h} (trigonal bipyramidal) compared to the often slightly electronically favored C_{4v} (square pyramidal) geometry,[70,71] thereby lending further support to drawing the sites as trigonal bipyramidal as one's initial working hypothesis. The catalyst poisoning steps in Scheme 7 are outside the catalytic cycle; hence, those steps are discussed in their own separate section later in this Discussion.

Critical in the active site structure drawn in Scheme 7 is the triazole N to Cu^{II} coordination shown, specifically triazole N-3 to Cu^{II} coordination. The favored active site in Figure 2 (*vide supra*) contains a cluster of 4 $Cu^{II}_{surface}$ sites comprising (1) two $Cu^{II}_{surface}$ sites coordinated by two N-2 atoms from separate BTTri linkers and (2) two $Cu^{II}_{surface}$ sites coordinated by two N-3 atoms from separate BTTri linkers. The active site drawn in Scheme 7 simplifies the structure in Figure 2 in that it shows only triazole N-3 to $Cu^{II}_{surface}$ coordination, only one coordinating triazole ring, and only one $Cu^{II}_{surface}$ site. While $Cu^{II}_{surface}$ sites coordinated by N-2 versus N-3 atoms may have slightly different electronic and geometric structures, our own previous work investigating the CuBTTri active sites shows that there is kinetically only a single type of active site.[22] Hence, if the hypothesized N-2 and N-3 coordinated $Cu^{II}_{surface}$ sites both catalyze GSNO to NO conversion, they do so with the same rate constant within experimental error and therefore likely via the same mechanistic pathway. What follows here is a brief list and description of each of the steps in Scheme 7.

Step 1) Rate constants k_1 and k_{-1}. Reversible coordination of GSH to Cu^{II} through sulfur displaces H_2O and initiates the catalytic cycle. Coordination from sulfur to formally Cu^{II} is represented using a dative bond formalism, that is, without a $-S^+-Cu^-$ charge implied in a valance bonding formalism, as that avoids the otherwise resultant confusion of an implied reduction to Cu^{I} (i.e., in a valance bonding oxidation-state formalism vs the traditional "even electron" Cu^{II} oxidation-state formalism utilized herein).[73] Step 1 forms a net neutral intermediate Cu site. Scheme 7 shows GSH coordination to Cu^{II} first for the sake of simplicity; however, it is possible that instead GSNO coordinates to Cu^{II} before GSH. Which species coordinates to Cu^{II} first could conceivably also vary with the relative concentrations of GSH/GSNO and would change the timing of steps in Scheme 7. The interested reader is directed to the Supporting Information for further details.

Step 2) Rate constants k_2 and k_{-2}. Reversible coordination of GSNO to Cu^{II} through nitrogen. Mechanisms analogous to Scheme 7 can be drawn where GSNO coordinates to Cu^{II} through sulfur. Overall, N vs S coordination of GSNO to Cu^{II} is a detail in the mechanism in Scheme 7 that will be addressed via future studies. The intermediate formed in Step 2 is a net −1 anionic complex.

Step 3) Rate constants k_3 and k_{-3}. Proposed intramolecular deprotonation of the thiol proton in GSH by the terminal carboxylate in GSH (Figure 1). The proposed

https://doi.org/10.1021/acscatal.2c00477
ACS Catal. 2022, 12, 8055−8068

proton relay accompanying PCET could occur via one or more H_2O molecules in a Grotthus-type proton hopping mechanism if the GSH tripeptide cannot coil sufficiently nor exactly for the terminal carboxylate group to meet the bound −SH moiety.[72] The deprotonation increases electron density around sulfur and Cu^{II}, and that helps drive the one electron transfer from S in GSH to N in GSNO. Critically, this PCET provides the driving force for homolysis of the S−N bond in GSNO and release of a thiyl radical (GS•). Step 3 is favorable in part because it results in the formation of a net neutral complex. Step 3 is also assumed to be the turnover-limiting step (t.l.s.), which means that $k_{-3} \ll k_4$ and k_5. Further support for the hypothesis that Step 3 is the t.l.s. is presented later in this Discussion section when analyzing the catalyst poisoning data in Figure 6 (*vide infra*). The concentration dependencies in the derived rate law for Scheme 7 (eq 6a) do not change if Steps 2, 3, 5, or 6 is set as the t.l.s., only the constants making up the net "k_{obs}" change. Hence, we present Step 3 as the t.l.s. at this time for the sake of simplicity and given point 4 discussed next.

Step 4) Rate constant k_4. Radical recombination of GS• to generate the GSSG product. Note that Step 4 is known to be diffusion-controlled, $>10^9$ s^{-1}, in H_2O for GS•.[62,74,75]

Step 5) Rate constants k_5 and k_{-5}. One e^- transfer from the formally $[NO]^-$ ligand to S in Cu^{II}-SG(CO_2H) is coupled to a reverse of the intramolecular deprotonation in Step 3, that is, sulfur ligand (SG) deprotonation of the terminal carboxylate group (i.e., SG-CO_2H). Electron transfer in Step 5 is proposed to result concomitant with a change in NO ligand geometry from bent (formally $[NO]^-$) to near-linear (formally •NO) driven by the higher reduction potential at S in GSH due to conversion of a formally −SG(CO_2H) ligand to a −S(***H***)G(CO_2^-) ligand. The intermediate formed retains the net neutral charge formed in Steps 3 and 4. The proposed catalytic cycle postulates that the CuBTTri catalyst utilizes what appears to be nature's elegant PCET chemistry for GS−NO bond activation.

Step 6) Rate constants k_6 and k_{-6}. Dissociation of NO from Cu^{II} and hence release of NO as the product results in regeneration of the Cu^{II} site generated in Step 1. It is possible of course that the intermediate shown in between Steps 5 and 6 is not needed, or at most a very transient species.

The derived rate law for the mechanism shown in Scheme 7, with k_3 as the t.l.s. when reaction pH = 4.5 (Supporting Information, Derivation S1), is given in eq 6a. This predicted equation for the mechanism in Scheme 7 matches the experimental rate law shown back in eq 5, where $k_{obs} = k_3 \times K_{eq,1} \times K_{eq,2}$.

$$\frac{-\mathrm{d[GSNO]}}{\mathrm{d}t} = k_3 K_{eq,1} K_{eq,2} [\mathrm{GSNO}][\mathrm{Cu}]_T [\mathrm{GSH(COO^-)}]^{1\rightarrow 0} \quad (6a)$$

The derived rate law for Scheme 7 when reaction pH > 4.5 also matches the experimental rate law shown in eq 4 (the full details can be found in Supporting Information, Derivation S1).

The mechanism in Scheme 7 can be written (by manipulating the coefficients of each elementary step) to sum to the experimentally observed reaction stoichiometry (Scheme 1). Previously, it was established that each equivalent of GSNO lost produced one equivalent of NO and one half of an equivalent of GSSG.[22] However, our previous work did not have an explanation for the disappearance of ∼15% of the GSH over the course of the reaction. The proposed mechanism in Scheme 7 explains part of the observed loss of GSH naturally, due to GSH bound to the Cu^{II} resting state of the catalyst. The loss of GSH may also occur by physisorption of GSH to CuBTTri over and above the binding of GSH to Cu^{II} (the active site being present at ∼1.3% of total Cu) as shown in Scheme 7.[75]

Understanding the pH-Dependent Results via the Deprotonation of Cu^{II}-S(*H*)G. When considering the −d[GSNO]/d*t* versus pH results in Figure 6, we were able to generate two reasonable hypotheses as to which proton(s) could be abstracted to result in the observed catalyst poisoning at alkaline pH: first, the thiol proton in GSH bound to a Cu^{II} site (Cu^{II}-S(***H***)G), and second, a protonated triazole moiety in BTTri bound to a Cu^{II} site (Cu^{II}-N_2(N**H**)C_2(N)). It is worth pointing out here that poisoning of Cu^{II} by OH^- can be ruled out because OH^- will react with the indicated pK_a ∼ 5.6 proton present at diffusion-controlled rates. Additionally, if OH^- were the kinetically dominant, direct poison, the data in Figure 6 would be expected to show a linear decline (or possibly an exponential decline) in the case of at least strong OH^- to Cu^{II} binding and not the observed sigmoidal curve and associated curve fit.

Scheme 7 shows the deprotonation of both Cu^{II}-S(***H***)G and Cu^{II}-N_2(N**H**)C_2(N) as possible pathways for $Cu^{II}_{surface}$ site poisoning. The Cu^{II}-S(***H***)G and Cu^{II}-N_2(N**H**)C_2(N) poisoning events are represented by the rate constants $k_{pois,GSH}$ and $k_{pois,tri}$ in Scheme 7, respectively. We hypothesize that mainly (or only) deprotonation of the Cu^{II}-S(**H**)G site in Scheme 7 is responsible for the loss of catalysis by CuBTTri observed at alkaline pH (Figure 6). The pK_a of the thiol proton in *unbound* GSH is ∼9.12, and the pK_a of the triazole proton in an *unbound* 1,2,3-triazole (such as H_3BTTri) is ∼9.3, hence almost the same.[61,76] Upon binding to the $Cu^{II}_{surface}$ site in CuBTTri, the pK_a value for the thiol proton in GSH should drop an estimated ∼2−4 orders of magnitude and fall between ∼5 and 7.[61] However, the pK_a value of Cu^{II}-N_2(N**H**)C_2(N) is expected to drop less than Cu^{II}-S(**H**)G because the protonated N-H is 4 bonds removed from Cu^{II} (as opposed to 2 bonds for Cu^{II}-S(**H**)G). Scheme 7 shows the triazole moiety in the protonated state (formally a neutral ligand) to reflect its likely protonation state at pH = 4.5. While one can write an analogous mechanism to Scheme 7 where the proton involved in PCET in Step 3 is Cu^{II}-N_2(N**H**)C_2(N) and not Cu^{II}-S(***H***)G (as currently written), Scheme 7 utilizes Cu^{II}-S(***H***)G for PCET for the sake of simplicity and because of proximity to the active site. However, the deprotonation of Cu^{II}-N_2(N**H**)C_2(N) cannot be unequivocally ruled out. In progress, computational work is aimed at addressing the deprotonation question of S-H versus N-H.

Scheme 7 proposes that the $Cu^{II}_{surface}$ site becomes poisoned upon abstraction of the Cu^{II}-S(***H***)G proton because removing the Cu^{II}-S(***H***)G proton before Step 2 of Scheme 7 can occur results in the formation of a thiolate ligand and a net −1 complex. Additionally, even if the net −1 site (Cu^{II}-(S^-)G) can still bind GSNO and then Step 3 of Scheme 7 still occurs, the catalytic cycle cannot be closed as written because there will be no proton available to couple with the electron transfer between the $[NO]^-$ ligand and the neutral S atom in Step 5 of Scheme 7.

https://doi.org/10.1021/acscatal.2c00477
ACS Catal. 2022, 12, 8055−8068

In short, PCET is proposed to be essential throughout the catalytic cycle.

The Question of a Formal Cu^{III} in Scheme 7. One alternative mechanistic hypothesis to Scheme 7, which cannot be conclusively disproven, generates the driving force for S−N bond homolysis via oxidation of Cu^{II} to formally Cu^{III} (Supporting Information, Scheme S3). The alternative Cu^{II} to Cu^{III} metal-based redox PCET mechanism exhibits the same reaction stoichiometry and derived rate law as Scheme 7 and drives catalysis via inner-sphere electron transfer directly between Cu^{II}/Cu^{III} and GSH/GSNO ligands. However, the Cu^{II}/Cu^{III} metal-based redox hypothesis is disfavored for the following reasons: Pauling's electroneutrality principle[77] states that the charge on the central metal ion in a complex lies between ±1 (others say ±0.5) and suggests that the formation of a truly Cu^{III} species is not likely. We are also aware of work that provides XAFS and DFT evidence that Cu^{III} physically probably does not exist in many cases.[78] Evidence against Cu^{III} formation is unsurprising considering Pauling's electroneutrality principle, the increasing effective nuclear charge on late first-row transition metals, and molecular orbital population analyses. In short, the formally Cu^{II} (and not Cu^{III}) species is written in Scheme 7 based on common oxidation-state formalisms currently in practice. Our intent is to show the general flow of electrons and associated arrow pushing that drives the key GS−NO bond cleavage step. The true charge on the central Cu ion is another matter, one we have no evidence for and hence no opinion on past what the current literature teaches.[49] Put another way, we wish to move past the long-standing issue of oxidation-state formalisms vs "true" charges on central metal ions and focus herein on the conceptual keys to the underlying chemically critical S−N bond cleavage reaction to medically useful NO• release. Some additional discussion of the formally Cu^{II}/Cu^{III} mechanism is provided in the Supporting Information for the interested reader. Another limiting case of a formal all Cu^{I} mechanism is also provided in the Supporting Information, a mechanism that, however, is currently disfavored as well for the same reasons other Cu^{I} mechanisms previously discussed are disfavored (*vide supra*).

Estimates of Thermodynamic and Kinetic Parameters in Scheme 7. One can estimate the parameters reported in Table 2 for Scheme 7 using the data in Figures 4 and 6 and the predicted rate laws given in Derivation S1 in the Supporting Information. What follows in this section is a brief discussion of how the parameters in Table 2 were estimated, with the full details in the Supporting Information.

Table 2. Estimated Reaction Parameters for Scheme 7 and the Kinetics Data Used to Calculate the Estimates[a]

reaction parameter	data used for estimation	value
$k_3 \times K_{eq,2}$ ($s^{-1}\ M^{-1}$)	Figure 4	$(5.6 \pm 1.6) \times 10^{-4}\ s^{-1}\ M^{-1}$
$K_{eq,1}$ (M^{-1})	Figure 4	$6.1\ M^{-1}$
$k_3 \times K_{eq,2}$ ($s^{-1}\ M^{-1}$)	Figure 6	$(5.01 \pm 0.4) \times 10^{-4}\ s^{-1}\ M^{-1}$
$K_{eq,pois}$ (M^{-1})	Figure 6	$(2.38 \pm 0.01) \times 10^{8}\ M^{-1}$

[a]The values for the apparent $K_{eq,1}$, $K_{eq,2}$, and $K_{eq,pois}$ parameters have dimensions as given (i.e., they are binding/reaction constants, not activity-based, dimensionless, true equilibrium constants).

The entries in Table 2 based on the data in Figure 4 were obtained as follows. The derived rate law for Scheme 7 when the reaction is 1st-order in [GSH] at pH = 4.5 is given above in eq 6a (reproduced below):

$$\frac{-\mathrm{d[GSNO]}}{\mathrm{d}t} = k_3 K_{eq,1} K_{eq,2} [\mathrm{GSNO}]^1 [\mathrm{Cu}]_T [\mathrm{GSH(COO^-)}]^{1\rightarrow 0} \quad (6b)$$

Therefore, the slope of the line in Figure 4 where the reaction is 1st-order in [GSH] is equal to $k_3 \times K_{eq,1} \times K_{eq,2} \times [\mathrm{Cu}]_T \times [\mathrm{GSNO}]$ ($[\mathrm{Cu}]_T$ and [GSNO] were held constant at 0.5 and 1 mM, respectively). Once the reaction is zero-order in [GSH] at pH = 4.5 the derived rate law simplifies to eq 7, as shown below, and $-\mathrm{d[GSNO]}/\mathrm{d}t$ becomes equal to a maximum constant value (as observed in Figure 4).

$$\frac{-\mathrm{d[GSNO]}}{\mathrm{d}t} = k_3 K_{eq,2} [\mathrm{GSNO}]^1 [\mathrm{Cu}]_T \quad (7)$$

Therefore, the constant value for $-\mathrm{d[GSNO]}/\mathrm{d}t$ in Figure 4 is equal to $k_3 \times K_{eq,2} \times [\mathrm{Cu}]_T \times [\mathrm{GSNO}]$, which yields the estimate for $k_3 \times K_{eq,2}$ in Table 2 using the data in Figure 4 (again with $[\mathrm{Cu}]_T$ and [GSNO] held constant at 0.5 and 1 mM, respectively). One can then calculate the estimate for $K_{eq,1}$ using the estimate for $k_3 \times K_{eq,2}$. Dividing the slope of the line in Figure 4 when the reaction is 1st-order in [GSH] by the estimate for $k_3 \times K_{eq,2}$ yields the estimate for $K_{eq,1}$ given in Table 2. The estimates for $K_{eq,1}$ and $k_3 \times K_{eq,2}$ given in Table 2 are physically reasonable: the association of GSH to Cu^{II} is mildly thermodynamically favorable ($K_{eq,1} = 6.1$), and the bulky thiol GSH is expected to be only a moderate ligand. The value for $k_3 \times K_{eq,2}$ ($(5.6 \pm 1.6) \times 10^{-4}\ s^{-1}$) is expected to be small and is consistent with the hypothesis that k_3 corresponds to the t.l.s. in Scheme 7.

The entries in Table 2 based on the data in Figure 6 were obtained as follows in brief (see the Supporting Information for full details). The derived rate law for Scheme 7 at pH ≥ 4.5 when the reaction is 0th-order in [GSH] (the conditions under which the data in Figure 6 were obtained) is given below in eq 8.

$$\left(\frac{-\mathrm{d[GSNO]}}{\mathrm{d}t}\right)_{\mathrm{pH}\geq 4.5} = \frac{k_3 K_{eq,2} [\mathrm{Cu}]_T [\mathrm{GSNO}]}{(1 + K_{eq,pois}[\mathrm{OH^-}])} \quad (8)$$

The value of the numerator of eq 8 is a constant, which can be denotaed a fit parameter, A. The value of $K_{eq,pois}$ in eq 8 is also a constant, which can be denoted a second a second fit parameter, B. We note here that the value of $K_{eq,pois}$ determined here is meant to represent a combination of the two equilibrium constants for the two separate poisoning events back in Scheme 7. The data in Figure 6 measures $-\mathrm{d[GSNO]}/\mathrm{d}t$ as a function of $[\mathrm{OH^-}]$ and therefore can be fit by an equation with the general form of eq 9, shown below, where $A = k_3 \times K_{eq,2} \times [\mathrm{Cu}]_T \times [\mathrm{GSNO}]$ and $B = K_{eq,pois}$.

$$y = \frac{A}{(1 + Bx)} \quad (9)$$

The fit of the data shown back in Figure 6 using eq 9 yields a second estimate for $k_3 \times K_{eq,2}$ from parameter A (as $[\mathrm{Cu}]_T$ and [GSNO] are known) and an estimate for $K_{eq,pois}$ from parameter B (both of which are reported in Table 2). The value of $k_3 \times K_{eq,2}$ estimated from the data in Figure 6 ($(5.0 \pm 0.4) \times 10^{-4}\ s^{-1}$) matches, within experimental error, the estimate for $k_3 \times K_{eq,2}$ from the data in Figure 4 ($(5.6 \pm 1.6) \times 10^{-4}\ s^{-1}$). The good agreement between these two estimates for $k_3 \times K_{eq,2}$ from two different sets of data supports the method of data collection, the

https://doi.org/10.1021/acscatal.2c00477
ACS Catal. 2022, 12, 8055−8068

treatment of the data and, overall, the proposed mechanism. The reasonably precise, if not accurate, estimation of $k_3 \times K_{eq,2}$ is also implied. The value estimated for $K_{eq,pois}$ from the data in Figure 6 is large, on the order of 10^8 according to the treatment in Figure 6. The large magnitude for $K_{eq,pois}$ is reasonable as the deprotonation in the poisoning step (Scheme 7) is energetically favorable (as the pK_a value of the thiol proton in GSH is expected to drop ~2−4 orders of magnitude compared to the unbound thiol)[79] and given that the resulting thiolate ligand is expected to be strongly bound to what is formally Cu^{II}. Note that successful fitting of kinetics data to obtain the reaction equilibrium and rate constant parameters in Table 2 is additional quantitative evidence that the mechanistic hypothesis in Scheme 7 is, at the very least, a decent initial mechanistic hypothesis consistent with and supported by the available data. Moreover, the equilibrium and rate constants obtained from fits of the kinetics data in Figures 4 and 6 to the predicted rate law(s) corresponding to Scheme 7 make physical sense (as discussed above), further supporting the reasonableness of the working mechanistic hypotheses presented as Scheme 7.

Possible Future Experiments Based on Predictions Derived from Scheme 7. A more reliable mechanism can both explain all the current data but also makes predictions that can be tested experimentally. The mechanism in Scheme 7 is no exception. Hence, some predictions based on the formally Cu^{II} Lewis acid, ligand-based redox PCET mechanism,[80,81] and possible future studies that go beyond the scope of this contribution, are detailed in the Supporting Information for the interested reader.

CONCLUSIONS

A novel PCET mechanism is proposed as the key behind the GS−NO bond homolysis catalyzed by CuBTTri (Scheme 7). Scheme 7 proposes that the key S−N bond homolysis in GSNO is driven by ligand-based PCET between the S atom in the GSH ligand and the N atom in the GSNO ligand. Scheme 7 proposes a mechanistic hypothesis where the Cu^{II} site does not undergo a change in at least formal oxidation state but, instead, primarily binds the GSH and GSNO ligands in a (Lewis acid) way that facilitates electron transfer between the S in Cu^{II}-S(*H*)G and the N in Cu^{II}-N(*O*)SG. The proposed mechanism satisfies the five minimum requirements listed in the Introduction for determining more reliable reaction mechanisms and explains the four primary experimental findings for the CuBTTri/GSNO/GSH/NO system listed at the end of the Results section. In short, Scheme 7 is offered as a minimum mechanistic working hypothesis for going forward, consistent with and supported by the currently available data.

The work reported herein is, to the best of our knowledge, a rare if not the first example where a proposed reaction mechanism for a MOF catalyst has been elucidated based upon (i) first establishing the active sites within the MOF and (ii) then also ensuring that the classic requirements for establishing a disproof-based, Ockham's razor obeying, hence more reliable reaction mechanism have been met.[49] Due to their exceptional chemical and physical tunability, MOF catalysts stand to benefit considerably from mechanistic insight for catalyst improvements and mechanism-directed catalyst design. Hence, it is hoped that the approach employed herein to elucidate the proposed PCET mechanism will prove of value to the communities connected to the MOF literature, biomedical NO generation, heterogeneous catalysis, and workers more generally interested in kinetic and mechanistic analyses of catalytic reactions.

ASSOCIATED CONTENT

Supporting Information

The Supporting Information is available free of charge at https://pubs.acs.org/doi/10.1021/acscatal.2c00477.

Powder X-ray diffraction pattern for CuBTTri, examining $-d[GSNO]/dt$ versus $[GSNO]_i$ at two concentrations, derivation for the rate law associated with Scheme 7, calculation of kinetic/thermodynamic parameters, two example limiting Cu^I mechanistic hypotheses, an example limiting Cu^{II}/Cu^{III} mechanistic hypothesis, disproven mechanistic hypotheses and analysis, ratio between thiolate and $Cu^{II}_{surface}$ at varying reaction pH, Scheme 7 apparent pK_a of the thiol proton in GSH bound to $Cu^{II}_{surface}$, and future experiments based on predictions derived from Scheme 7 (PDF)

AUTHOR INFORMATION

Corresponding Authors

Richard G. Finke − *Department of Chemistry, Colorado State University, Fort Collins, Colorado 80523, United States*; Email: richard.finke@colostate.edu

Melissa M. Reynolds − *Department of Chemistry, School of Biomedical Engineering, and Department of Chemical & Biological Engineering, Colorado State University, Fort Collins, Colorado 80523, United States*; orcid.org/0000-0002-1836-7324; Email: melissa.reynolds@colostate.edu

Author

Robert R. Tuttle − *Department of Chemistry, Colorado State University, Fort Collins, Colorado 80523, United States*

Complete contact information is available at: https://pubs.acs.org/10.1021/acscatal.2c00477

Notes

The authors declare no competing financial interest.

ACKNOWLEDGMENTS

This research was supported by the NSF under Career Award #1352201 and by NSF Grant #1664646, the latter for R.G.F.'s time and contributions. The authors thank the Central Instrument Facility (CIF) scientists at CSU and especially Dr. Chris Rithner for help with the ^{1}H NMR data acquisition. The authors thank the members of M.M.R.'s and R.G.F.'s research groups for several readings of this manuscript in different versions and their always critical, constructive feedback.

REFERENCES

(1) Harding, J. L.; Reynolds, M. M. Metal Organic Frameworks as Nitric Oxide Catalysts. *J. Am. Chem. Soc.* **2012**, *134*, 3330−3333.

(2) Harding, J. L.; Metz, J. M.; Reynolds, M. M. A Tunable, Stable, and Bioactive MOF Catalyst for Generating a Localized Therapeutic from Endogenous Sources. *Adv. Funct. Mater.* **2014**, *24*, 7503−7509.

(3) Liu, K.; Meyerhoff, M. E. Preparation and Characterization of an Improved Cu2+−Cyclen Polyurethane Material That Catalyzes Generation of Nitric Oxide from S-Nitrosothiols. *J. Mater. Chem.* **2012**, *22*, 18784−18787.

(4) Ren, H.; Wu, J.; Xi, C.; Lehnert, N.; Major, T.; Bartlett, R. H.; Meyerhoff, M. E. Electrochemically Modulated Nitric Oxide (NO) Releasing Biomedical Devices via Copper(II)-Tri(2-Pyridylmethyl)-

Amine Mediated Reduction of Nitrite. *ACS Appl. Mater. Interfaces* **2014**, *6*, 3779−3783.
(5) White, C. J.; Lehnert, N.; Meyerhoff, M. E. Electrochemical Generation of Nitric Oxide for Medical Applications. *Electrochem. Sci. Adv.* **2021**, No. e2100156.
(6) Mengel, A.; Lindermayer, C. *Nitric Oxide: Methods and Protocols*; Springer: New York, 2018, DOI: 10.1007/978-1-4939-7695-9.
(7) Marletta, M. A. Nitric Oxide: Biosynthesis and Biological Significance. *Trends Biochem. Sci.* **1989**, *14*, 488−492.
(8) Coleman, J. W. Nitric Oxide in Immunity and Inflammation. *Int. Immunopharmacol.* **2001**, *1*, 1397−1406.
(9) Bogdan, C. Nitric Oxide and the Immune Response. *Nat. Immunol.* **2001**, *2*, 907−916.
(10) Carpenter, A. W.; Schoenfisch, M. H. Nitric Oxide Release: Part II. Therapeutic Applications. *Chem. Soc. Rev.* **2012**, *41*, 3742−3752.
(11) Knott, A. B.; Bossy-Wetzel, E. Nitric Oxide in Health and Disease of the Nervous System. *Antioxid. Redox Signaling* **2009**, *11*, 541−553.
(12) Schairer, D. O.; Chouake, J. S.; Nosanchuk, J. D.; Friedman, A. J. The Potential of Nitric Oxide Releasing Therapies as Antimicrobial Agents. *Virulence* **2012**, *3*, 271−279.
(13) Neufeld, B. H.; Reynolds, M. M. Critical Nitric Oxide Concentration for Pseudomonas Aeruginosa Biofilm Reduction on Polyurethane Substrates. *Biointerphases* **2016**, *11*, 31012.
(14) Paricio, L.; Neufeld, B.; Reynolds, M. Combined Influence of Nitric Oxide and Surface Roughness in Biofilm Reduction across Bacteria Strains. *Biointerphases* **2019**, *14*, 21004.
(15) Palmer, R. M. J.; Ferrige, A. G.; Moncada, S. Nitric Oxide Release Accounts for the Biological Activity of Endothelium-Derived Relaxing Factor. *Nature* **1987**, *327*, 524−526.
(16) Neufeld, M. J.; Lutzke, A.; Jones, W. M.; Reynolds, M. M. Nitric Oxide Generation from Endogenous Substrates Using Metal−Organic Frameworks: Inclusion within Poly(Vinyl Alcohol) Membranes To Investigate Reactivity and Therapeutic Potential. *ACS Appl. Mater. Interfaces* **2017**, *9*, 35628−35641.
(17) Singh, S. P.; Wishnok, J. S.; Keshive, M.; Deen, W. M.; Tannenbaum, S. R. The Chemistry of the S-Nitrosoglutathione/Glutathione System. *Proc. Natl. Acad. Sci. U. S. A.* **1996**, *93*, 14428−14433.
(18) Broniowska, K. A.; Diers, A. R.; Hogg, N. S-Nitrosoglutathione. *Biochim. Biophys. Acta* **2013**, *1830*, 3173−3181.
(19) Noble, D.; Swift, H.; Lyn, H.; Williams, D. Nitric Oxide Release from S-Nitrosoglutathione (GSNO). *Chem. Commun.* **1999**, *22*, 2317−2318.
(20) Gorren, A. C. F.; Schrammel, A.; Schmidt, K.; Mayer, B. Decomposition OfS-Nitrosoglutathione in the Presence of Copper Ions and Glutathione. *Arch. Biochem. Biophys.* **1996**, *330*, 219−228.
(21) Tsikas, D.; Schmidt, M.; Böhmer, A.; Zoerner, A. A.; Gutzki, F.-M.; Jordan, J. UPLC-MS/MS Measurement of S-Nitrosoglutathione (GSNO) in Human Plasma Solves the S-Nitrosothiol Concentration Enigma. *J. Chromatogr., B: Anal. Technol. Biomed. Life Sci.* **2013**, *927*, 147−157.
(22) Tuttle, R. R.; Rubin, H. N.; Rithner, C. D.; Finke, R. G.; Reynolds, M. M. Copper Ion vs Copper Metal−Organic Framework Catalyzed NO Release from Bioavailable S-Nitrosoglutathione En Route to Biomedical Applications: Direct 1H NMR Monitoring in Water Allowing Identification of the Distinct, True Reaction Stoichiometries and Thio. *J. Inorg. Biochem.* **2019**, *199*, No. 110760.
(23) Tuttle, R.; Folkman, S. J.; Rubin, H. N.; Finke, R. G.; Reynolds, M. Copper Metal−Organic Framework Surface Catalysis: Catalyst Poisoning, IR Spectroscopic, and Kinetic Evidence Addressing the Nature and Number of the Catalytically Active Sites En Route to Improved Applications. *ACS Appl. Mater. Interfaces* **2020**, *0*, 39043.
(24) Neufeld, M. J.; Ware, B. R.; Lutzke, A.; Khetani, S. R.; Reynolds, M. M. Water-Stable Metal−Organic Framework/Polymer Composites Compatible with Human Hepatocytes. *ACS Appl. Mater. Interfaces* **2016**, *8*, 19343−19352.
(25) Baciu, C.; Cho, K.-B.; Gauld, J. W. Influence of Cu+ on the RS-NO Bond Dissociation Energy of S-Nitrosothiols. *J. Phys. Chem. B* **2005**, *109*, 1334−1336.
(26) Dicks, A. P.; Swift, H. R.; Williams, D. L. H.; Butler, A. R.; Al-Sadoni, H. H.; Cox, B. G. Identification of Cu+ as the Effective Reagent in Nitric Oxide Formation from S-Nitrosothiols (RSNO). *J. Chem. Soc., Perkin Trans. 2* **1996**, *4*, 481−487.
(27) Tuttle, R. R.; Daly, R. E.; Rithner, C. D.; Reynolds, M. M. Monitoring a MOF Catalyzed Reaction Directly in Blood Plasma. *ACS Appl. Mater. Interfaces* **2021**, 52006.
(28) Dincă, M.; Long, J. R. High-Enthalpy Hydrogen Adsorption in Cation-Exchanged Variants of the Microporous Metal−Organic Framework Mn3[(Mn4Cl)3(BTT)8(CH3OH)10]2. *J. Am. Chem. Soc.* **2007**, *129*, 11172−11176.
(29) Demessence, A.; D'Alessandro, D. M.; Foo, M. L.; Long, J. R. Strong CO2 Binding in a Water-Stable, Triazolate-Bridged Metal−Organic Framework Functionalized with Ethylenediamine. *J. Am. Chem. Soc.* **2009**, *131*, 8784−8786.
(30) Dincă, M.; Han, W. S.; Liu, Y.; Dailly, A.; Brown, C. M.; Long, J. R. Observation of Cu2+−H2 Interactions in a Fully Desolvated Sodalite-Type Metal−Organic Framework. *Angew. Chem., Int. Ed.* **2007**, *46*, 1419−1422.
(31) Metzger, E. D.; Comito, R. J.; Hendon, C. H.; Dincă, M. Mechanism of Single-Site Molecule-Like Catalytic Ethylene Dimerization in Ni-MFU-4l. *J. Am. Chem. Soc.* **2017**, *139*, 757−762.
(32) Dicks, A. P.; Herves Beloso, P.; Lyn, H.; Williams, D. Decomposition of S-Nitrosothiols: The Effects of Added Thiols. *J. Chem. Soc., Perkin Trans. 2* **1997**, *8*, 1429−1434.
(33) Marcus, R. A. Chemical and Electrochemical Electron-Transfer Theory. *Annu. Rev. Phys. Chem.* **1964**, *15*, 155−196.
(34) Bernasconi, C. F. Intrinsic Barriers of Reactions and the Principle of Nonperfect Synchronization. *Acc. Chem. Res.* **1987**, *20*, 301−308.
(35) Hornstein, B. J.; Aiken, J. D.; Finke, R. G. Nanoclusters in Catalysis: A Comparison of CS2 Catalyst Poisoning of Polyoxoanion- and Tetrabutylammonium-Stabilized 40 ± 6 Å Rh(0) Nanoclusters to 5 Rh/Al2O3, Including an Analysis of the Literature Related to the CS2 to Metal Stoichiometry Issue. *Inorg. Chem.* **2002**, *41*, 1625−1638.
(36) Gascon, J.; Corma, A.; Kapteijn, F.; Llabrési i Xamena, F. X. Metal Organic Framework Catalysis: Quo Vadis? *ACS Catal.* **2014**, *4*, 361−378.
(37) Yang, D.; Gates, B. C. Catalysis by Metal Organic Frameworks: Perspective and Suggestions for Future Research. *ACS Catal.* **2019**, *9*, 1779−1798.
(38) Danilina, N.; Krumeich, F.; Castelanelli, S. A.; van Bokhoven, J. A. Where Are the Active Sites in Zeolites? Origin of Aluminum Zoning in ZSM-5. *J. Phys. Chem. B* **2010**, *114*, 6640−6645.
(39) Behrens, M.; Studt, F.; Kasatkin, I.; Kähl, S.; Hävecker, M.; Abild-Pedersen, F.; Zander, S.; Girgsdies, F.; Kurr, P.; Kniep, B.-L.; Tovar, M.; Fischer, R. W.; Nørskov, J. K.; Schlögl, R. The Active Site of Methanol Synthesis over Cu/ZnO/2O3 Industrial Catalysts. *Science* **2012**, *336*, 893−897.
(40) Bayram, E.; Finke, R. G. Quantitative 1,10-Phenanthroline Catalyst-Poisoning Kinetic Studies of Rh(0) Nanoparticle and Rh4 Cluster Benzene Hydrogenation Catalysts: Estimates of the Poison Kassociation Binding Constants, of the Equivalents of Poison Bound and of the Number of Cata. *ACS Catal.* **2012**, *2*, 1967−1975.
(41) Hagen, C. M.; Vieille-Petit, L.; Laurenczy, G.; Süss-Fink, G.; Finke, R. G. Supramolecular Triruthenium Cluster-Based Benzene Hydrogenation Catalysis: Fact or Fiction? *Organometallics* **2005**, *24*, 1819−1831.
(42) Bayram, E.; Lu, J.; Aydin, C.; Uzun, A.; Browning, N. D.; Gates, B. C.; Finke, R. G. Mononuclear Zeolite-Supported Iridium: Kinetic, Spectroscopic, Electron Microscopic, and Size-Selective Poisoning Evidence for an Atomically Dispersed True Catalyst at 22 °C. *ACS Catal.* **2012**, *2*, 1947−1957.
(43) Bayram, E.; Linehan, J. C.; Fulton, J. L.; Roberts, J. A. S.; Szymczak, N. K.; Smurthwaite, T. D.; Özkar, S.; Balasubramanian, M.; Finke, R. G. Is It Homogeneous or Heterogeneous Catalysis Derived from [RhCp*Cl2]2? In Operando XAFS, Kinetic, and Crucial Kinetic Poisoning Evidence for Subnanometer Rh4 Cluster-Based Benzene Hydrogenation Catalysis. *J. Am. Chem. Soc.* **2011**, *133*, 18889−18902.

https://doi.org/10.1021/acscatal.2c00477
ACS Catal. 2022, 12, 8055−8068

(44) Chen, X.; Lyu, Y.; Wang, Z.; Qiao, X.; Gates, B. C.; Yang, D. Tuning Zr12O22 Node Defects as Catalytic Sites in the Metal−Organic Framework Hcp UiO-66. *ACS Catal.* **2020**, *10*, 2906−2914.
(45) Yang, D.; Ortuño, M. A.; Bernales, V.; Cramer, C. J.; Gagliardi, L.; Gates, B. C. Structure and Dynamics of Zr6O8 Metal−Organic Framework Node Surfaces Probed with Ethanol Dehydration as a Catalytic Test Reaction. *J. Am. Chem. Soc.* **2018**, *140*, 3751−3759.
(46) Simons, M. C.; Vitillo, J. G.; Babucci, M.; Hoffman, A. S.; Boubnov, A.; Beauvais, M. L.; Chen, Z.; Cramer, C. J.; Chapman, K. W.; Bare, S. R.; Gates, B. C.; Lu, C. C.; Gagliardi, L.; Bhan, A. Structure, Dynamics, and Reactivity for Light Alkane Oxidation of Fe(II) Sites Situated in the Nodes of a Metal−Organic Framework. *J. Am. Chem. Soc.* **2019**, *141*, 18142−18151.
(47) Watzky, M. A.; Finke, R. G. Pseudoelementary Steps: A Key Concept and Tool for Studying the Kinetics and Mechanisms of Complex Chemical Systems. *J. Phys. Chem. A* **2021**, *125*, 10687−10705.
(48) Scott, S. L. The Burden of Disproof. *ACS Catal.* **2019**, *9*, 4706−4708.
(49) Hoffman, R.; Minkin, V. I.; Carpenter, B. K. Ockham's Razor and Chemistry. *Int. J. Philos. Chem.* **1997**, *3*, 3−28.
(50) Bligaard, T.; Bullock, R. M.; Campbell, C. T.; Chen, J. G.; Gates, B. C.; Gorte, R. J.; Jones, C. W.; Jones, W. D.; Kitchin, J. R.; Scott, S. L. Toward Benchmarking in Catalysis Science: Best Practices, Challenges, and Opportunities. *ACS Catal.* **2016**, *6*, 2590−2602.
(51) Xiao, D. J.; Oktawiec, J.; Milner, P. J.; Long, J. R. Pore Environment Effects on Catalytic Cyclohexane Oxidation in Expanded Fe2(Dobdc) Analogues. *J. Am. Chem. Soc.* **2016**, *138*, 14371−14379.
(52) Kaur, G.; Øien-Ødegaard, S.; Lazzarini, A.; Chavan, S. M.; Bordiga, S.; Lillerud, K. P.; Olsbye, U. Controlling the Synthesis of Metal−Organic Framework UiO-67 by Tuning Its Kinetic Driving Force. *Cryst. Growth Des.* **2019**, *19*, 4246−4251.
(53) Furukawa, H.; Müller, U.; Yaghi, O. M. "Heterogeneity within Order" in Metal−Organic Frameworks. *Angew. Chem., Int. Ed.* **2015**, *54*, 3417−3430.
(54) Furukawa, H.; Cordova, K. E.; O'Keeffe, M.; Yaghi, O. M. The Chemistry and Applications of Metal-Organic Frameworks. *Science* **2013**, *341*, 1230444.
(55) Moosavi, S. M.; Nandy, A.; Jablonka, K. M.; Ongari, D.; Janet, J. P.; Boyd, P. G.; Lee, Y.; Smit, B.; Kulik, H. J. Understanding the Diversity of the Metal-Organic Framework Ecosystem. *Nat. Commun.* **2020**, *11*, 4068.
(56) Hart, T. W. Some Observations Concerning the S-Nitroso and S-Phenylsulphonyl Derivatives of L-Cysteine and G. *Tetrahedron Lett.* **1985**, *26*, 2013−2016.
(57) Wang, C.; Wang, J.-L.; Lin, W. Elucidating Molecular Iridium Water Oxidation Catalysts Using Metal−Organic Frameworks: A Comprehensive Structural, Catalytic, Spectroscopic, and Kinetic Study. *J. Am. Chem. Soc.* **2012**, *134*, 19895−19908.
(58) Notheisz, F.; Zsigmond, A.; Bartók, M.; Szegletes, Z.; Smith, G. Mass Transfer Test and Maximum Rate Determination during Liquid-Phase Hydrogenations. *Appl. Catal., A* **1994**, *120*, 105−114.
(59) Simpson, A. J.; Brown, S. A. Purge NMR: Effective and Easy Solvent Suppression. *J. Magn. Reson.* **2005**, *175*, 340−346.
(60) Abeles, R.; Frey, P.; Jencks, W. *Biochemistry*; 1992.
(61) Tummanapelli, A. K.; Vasudevan, S. Ab Initio MD Simulations of the Brønsted Acidity of Glutathione in Aqueous Solutions: Predicting PKa Shifts of the Cysteine Residue. *J. Phys. Chem. B* **2015**, *119*, 15353−15358.
(62) Ngamchuea, K.; Batchelor-McAuley, C.; Compton, R. G. The Copper(II)-Catalyzed Oxidation of Glutathione. *Chem. − Eur. J.* **2016**, *22*, 15937−15944.
(63) Keszler, A.; Zhang, Y.; Hogg, N. Reaction between Nitric Oxide, Glutathione, and Oxygen in the Presence and Absence of Protein: How Are S-Nitrosothiols Formed? *Free Radical Biol. Med.* **2010**, *48*, 55−64.
(64) Williams, D. L. H. The Chemistry of S-Nitrosothiols. *Acc. Chem. Res.* **1999**, *32*, 869−876.
(65) Singh, R. J.; Hogg, N.; Joseph, J.; Kalyanaraman, B. Mechanism of Nitric Oxide Release from S-Nitrosothiols. *J. Biol. Chem.* **1996**, *271*, 18596−18603.
(66) Askew, S. C.; Barnett, D. J.; McAninly, J.; Williams, D. L. H. Catalysis by Cu2+ of Nitric Oxide Release from S-Nitrosothiols (RSNO). *J. Chem. Soc., Perkin Trans. 2* **1995**, *4*, 741−745.
(67) Lehnert, N.; Kim, E.; Dong, H. T.; Harland, J. B.; Hunt, A. P.; Manickas, E. C.; Oakley, K. M.; Pham, J.; Reed, G. C.; Alfaro, V. S. The Biologically Relevant Coordination Chemistry of Iron and Nitric Oxide: Electronic Structure and Reactivity. *Chem. Rev.* **2021**, *121*, 14682−14905.
(68) Zhang, S.; Çelebi-Ölçüm, N.; Melzer, M. M.; Houk, K. N.; Warren, T. H. Copper(I) Nitrosyls from Reaction of Copper(II) Thiolates with S-Nitrosothiols: Mechanism of NO Release from RSNOs at Cu. *J. Am. Chem. Soc.* **2013**, *135*, 16746−16749.
(69) Burg, A.; Cohen, H.; Meyerstein, D. The Reaction Mechanism of Nitrosothiols with Copper(I). *JBIC J. Biol. Inorg. Chem.* **2000**, *5*, 213−217.
(70) Xiang, J. Y.; Ponder, J. W. An Angular Overlap Model for Cu(II) Ion in the AMOEBA Polarizable Force Field. *J. Chem. Theory Comput.* **2014**, *10*, 298−311.
(71) Suta, M.; Cimpoesu, F.; Urland, W. The Angular Overlap Model of Ligand Field Theory for f Elements: An Intuitive Approach Building Bridges between Theory and Experiment. *Coord. Chem. Rev.* **2021**, *441*, 213981.
(72) Agmon, N. The Grotthuss Mechanism. *Chem. Phys. Lett.* **1995**, *244*, 456−462.
(73) Jack, R.; Finke, R. G.; Collman, J. P.; Xanne Stehr, R. *Principles and Applications of Organotransition Metal Chemistry*; University Science Books, 1987.
(74) Homer, N. Z. M.; Reglinski, J.; Sowden, R.; Spickett, C. M.; Wilson, R.; Walker, J. J. Dimethylsulfoxide Oxidizes Glutathione in Vitro and in Human Erythrocytes: Kinetic Analysis by 1H NMR. *Cryobiology* **2005**, *50*, 317−324.
(75) Jones, W. M.; Tapia, J. B.; Tuttle, R. R.; Reynolds, M. M. Thermogravimetric Analysis and Mass Spectrometry Allow for Determination of Chemisorbed Reaction Products on Metal Organic Frameworks. *Langmuir* **2020**, *36*, 3903.
(76) Baran, R. *Essentials of Heterocyclic Chemistry-I* https://www.scripps.edu/baran/heterocycles/Essentials1-2009.pdf.
(77) Pauling, L. *The Nature of the Chemical Bond*, 3rd ed.; Cornell University Press, 1960.
(78) DiMucci, I. M.; Lukens, J. T.; Chatterjee, S.; Carsch, K. M.; Titus, C. J.; Lee, S. J.; Nordlund, D.; Betley, T. A.; MacMillan, S. N.; Lancaster, K. M. The Myth of D8 Copper(III). *J. Am. Chem. Soc.* **2019**, *141*, 18508−18520.
(79) Graminski, G. F.; Kubo, Y.; Armstrong, R. N. Spectroscopic and Kinetic Evidence for the Thiolate Anion of Glutathione at the Active Site of Glutathione S-Transferase. *Biochemistry* **1989**, *28*, 3562−3568.
(80) Hammes-Schiffer, S. Theoretical Perspectives on Proton-Coupled Electron Transfer Reactions. *Acc. Chem. Res.* **2001**, *34*, 273−281.
(81) Hammes-Schiffer, S.; Stuchebrukhov, A. A. Theory of Coupled Electron and Proton Transfer Reactions. *Chem. Rev.* **2010**, *110*, 6939−6960.

https://doi.org/10.1021/acscatal.2c00477
ACS Catal. 2022, 12, 8055−8068